Rational Design of a Transferrin-Binding Peptide Sequence Tailored to Targeted Nanoparticle Internalization

M. Santi, [a,1,2]* G. Maccari,[a, 1] P. Mereghetti,[1] V.Voliani,[1] S. Rocchiccioli,[3] N. Ucciferri,[3] S.Luin,[2] G. Signore[1]*

[1]Center for Nanotechnology Innovation@NEST, Istituto Italiano di Tecnologia, Piazza San Silvestro 12, Pisa 56127, Italy. [2] NEST, Scuola Normale Superiore and Istituto Nanoscienze-CNR, Piazza San Silvestro 12, Pisa 56127, Italy. [3]Institute of Clinical Physiology-CNR, Via Giuseppe Moruzzi 1, Pisa 56124, Italy.

[a] Equal contribution

Corresponding author: Email: Giovanni.signore@iit.it, Melissa.santi@sns.it

Published version: https://pubs.acs.org/doi/full/10.1021/acs.bioconjchem.6b00611#

The transferrin receptor (TfR) is a promising target in cancer therapy owing to its overexpression in most solid tumors and on the blood brain barrier. Nanostructures chemically derivatized with transferrin are employed in TfR targeting but often lose their functionality upon injection in the bloodstream. As an alternative strategy, we rationally designed a peptide coating able to bind transferrin on suitable pockets not involved in binding to TfR or iron, by using an iterative multiscale-modeling approach coupled with Quantitative Structure-Activity and Relationship (QSAR) analysis and evolutionary algorithms. We tested that selected sequences have low aspecific protein adsorption and high binding energy towards transferrin, and one of them is efficiently internalized in cells with a transferrin-dependent pathway. Furthermore, it promotes transferrin-mediated endocytosis of gold nanoparticles by modifying their protein corona and promoting oriented adsorption of transferrin. This strategy leads to highly effective nanostructures, potentially useful in diagnostic and therapeutic applications, which exploit -and do not suffer- the protein solvation for achieving a better targeting.

Keywords: Transferrin, nanoparticles, targeted delivery, protein corona, rational design

INTRODUCTION

The use of targeted delivery systems able to convey a molecular payload in diseased tissues is one of the most ambitious goals of current nanomedicine research. Nanostructured materials play a pivotal role in this field, owing to their straightforward surface derivatization, high loading capability, and intriguing potential as contrast agents *in vivo*.[1] Selectivity towards specific pathologic tissues can be conferred by covalent decoration with proteins[2], antibodies,[3] aptamers,[4,5] and small ligands,[6] which recognize receptors differentially expressed between pathologic and healthy tissues. This strategy, however, often leads to unsatisfying results *in vivo*, owing to the high free energy of nanoparticles surface that promote the formation of a protein shell (the "protein corona")[7] which solvates the nanostructure upon injection in the bloodstream. The structure and the composition of the protein corona depends on the physico-chemical properties of nanoparticles like size, shape, colloidal stability, surface charge and its distribution.[8] Because of the presence of this biological milieu, nanoparticles may lose specificity and targeting capabilities of the functional groups on their surface, thus reducing or modifying cellular uptake.[9]

An elegant alternative is represented by the modulation of the protein corona composition, which leads to nanostructures that acquire selectivity directly in the bloodstream.[10] This strategy requires ligands that bind specific serum proteins without altering their biological function. Indeed, the effect of this "protein corona" modulation could confer intriguing homing properties to nanostructured systems, which are particularly susceptible of serum protein solvation and could better exploit the presence of an actively targeting protein shell. How to select these sequences, however, remains challenging. Empirical approaches such as phage display, yeast-two-hybrid, and Systematic Evolution of Ligands by Exponential Enrichment (SELEX) would provide unsatisfactory results, due to the unpredictable binding site on the target protein, which could lose its biological function.[11,12] Additionally, these techniques require relatively large amounts of target protein, which can be difficult to produce. Conversely, computationally driven design can provide ligand sequences able to recognize selectively a specific non-binding domain of the target protein, leaving unaltered its biological function. Transferrin receptor (TfR) is a trans-membrane protein formed by two subunits that mediate iron transport and cell growth regulation. Each subunit can bind one transferrin (Tf) molecule loaded with two iron ions that are internalized exploiting clathrin-mediated endocytosis.[13] TfR is ubiquitously expressed at low levels in human tissues,[14] and highly overexpressed in proliferating cells. It is commonly accepted that TfR expression is correlated with tumor progression,[15] and its expression on the surface of tumor cells makes TfR a therapeutic target for solid tumors treatment.[16] Furthermore, it plays a principal role in promoting translocation of iron across the blood brain barrier, and is a promising "Trojan horse" to perform delivery to the brain of otherwise non-permeant structures. Its natural ligand transferrin (Tf) has been exploited for delivery of small drugs,[17,18] toxins,[19] enzymes,[20] and nucleic acids.[21] Tf is present at high concentrations in blood, and represents an ideal target for the validation of our rational design strategy. Here, we show the results on the rational development and *in vitro* evaluation of transferrin-binding peptides.

RESULTS AND DISCUSSION

Rational design of transferrin-binding peptides

First, we developed a generic method for the virtual screening of peptide docking using Martini Coarse Grained (CG)[22] force field for protein. The method (Figure 1A) consists of an iterative procedure that combines the use of bash script, python, java, and GROMACS tools to automatically dig in the sequence the space for the optimal docking of peptide. Starting from the crystal structure of diferric transferrin (3V83A),[23] we identified using the Fpocket webserver[24] five potential binding sites (Figure 1B). Selection of the most appropriate binding pocket was performed with two aims in mind: the ideal pocket should be large enough to accommodate a peptide, and should not be near the binding site for the transferrin receptor or for iron. The first requirement allows selecting sequences with sufficiently high

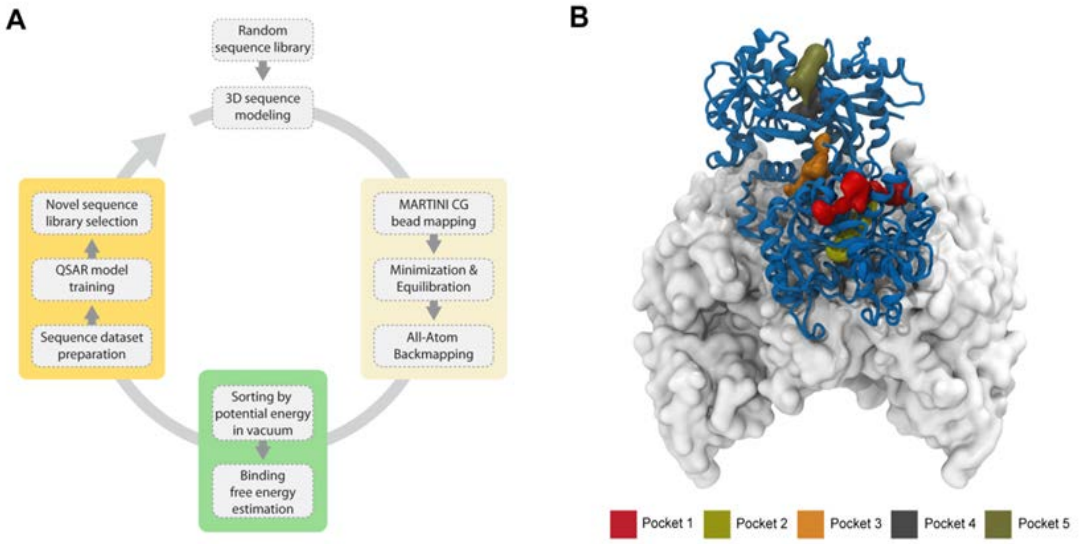

Figure 1. Virtual screening method. A) Diagram showing the steps for the virtual screening. B) Pockets identified on the human transferrin. Transferrin is represented with the blue ribbon diagram, part of the ectodomain of the transferrin receptor dimer[23] is rendered by its accessible surface. Pocket 3 (orange) is the one chosen to dock the peptide on the bases of the available volume and on the distance from the iron binding site.

affinity, while the second should minimize interference of potentially bulky payloads on binding processes to TfR and iron ions. These requirements led to the choice of Pocket 3 (Figure 1B) as the most appropriate site, and preliminary measurements suggested that this site could accommodate up to six amino acids. This is a sufficiently long sequence to provide good binding affinity and selectivity, yet short enough to allow exploring a reasonable number of combinations. Our strategy involves several computational steps in which a mathematical model describing the physico-chemical requirements for binding is inferred from molecular dynamics simulation data. In this iterative procedure, a set of peptide sequences is generated at each step and the linear 3D structure of each peptide is built and placed within the binding pocket. The peptide is docked using coarse grained molecular dynamics simulations (Figure 2A). The free binding energy of the docked poses is estimated using the molecular mechanics Poisson-Boltzmann surface area (MM-PBSA) method.[25] To design new candidates for the next iterative step, each peptide sequence is encoded into a number of descriptors related to its physico-chemical features and associated to the theoretical binding energy (Table S1). A regression model is then inferred by combining the encoded information from all the previous steps, thus obtaining at each iteration a mathematical model that better perceives bioactive sequences. The regression model is combined to multi-objective evolutional algorithms (MOEA) to design candidate sequences for the next iteration with optimal properties. In this phase, sequence optimization is carried out with two different objectives: having the lowest binding free energy, and the lowest number of charged/hydrophobic sequences (Figure 2B). The last requirement accounts for the need to limit aspecific adsorption to serum proteins, which is particularly relevant for positively charged or highly hydrophobic structures. The algorithm resulted in a distributed population of binding peptides, with some candidate sequences that better fit the requirement of high binding and low net charge/hydrophobicity. In fact, the MOEA does not identify the best solution, but a set of sub optimal solutions at the given problem. The entire procedure (sequence design, docking, scoring) were repeated iteratively (Figure 2B). The top three peptides (Tf1, Tf2, Tf3) designed by the MOEA at the last iteration were selected for experimental evaluation, along with a scrambled version of Tf2 acting as control sequence.

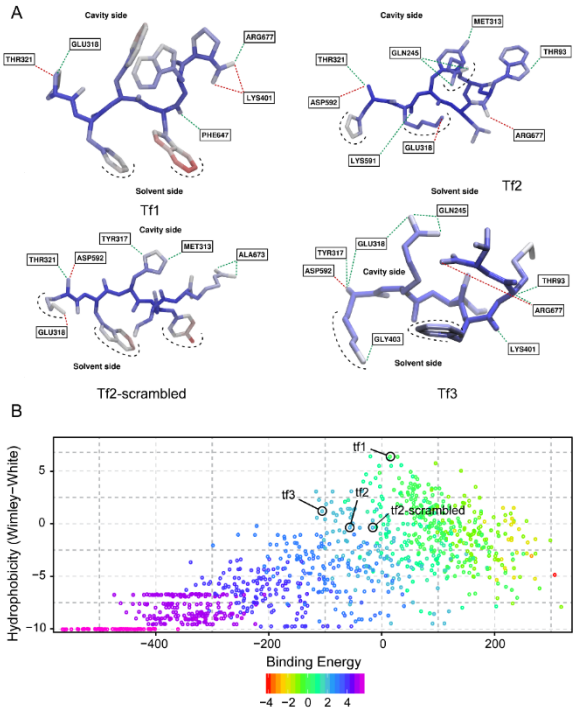

Figure 2: A) Three dimensional docked poses. Representative docked poses, obtained from a cluster analysis of equilibrium all-atoms trajectories, for Tf1, Tf2, Tf2-scrambled, and Tf3 (see Method Section). Hydrogen bonds (green dashed lines) and salt bridges (red dashed lines) formed between the peptide and the amino acids in the Tf1 pocket are shown. Atoms are colored according to their root mean squared displacement, blue: rigid regions, red: flexible regions. Black dashed lines highlight solvent exposed atoms. B) Results of the virtual screening, showing the distribution of the theoretical binding energy versus peptide hydrophobicity measured with the combined consensus hydrophobicity scale (CCS).[26,27] Color scale represents peptides net charge at pH 7 (red: negative, magenta: positive).

Quartz Crystal Microbalance with Dissipation Monitoring (QCM-D) measurements

We synthesized the selected peptides (Tf1, Tf2, Tf3, and Tf2scr, Table 1) by standard solid phase synthesis. All the sequences were provided with a spacer (GGG) with an N-terminal cysteine, to allow conjugation with fluorescent reporters or binding to gold-coated surfaces without hampering binding with Tf. We then evaluated Tf binding affinity of Tf1, Tf2, and Tf3 by measures with a quartz crystal microbalance (QCM-D). Peptides were immobilized on a gold sensor and increasing concentrations of human Tf were injected sequentially (Fig S1). The resonance frequency shift was used to calculate the binding constant (Ka) and its reciprocal (Kd) using Langmuir equation.

Table 1: Dissociation constants obtained from quartz-crystal microbalance measurements using transferrin and BSA at 25 °C in PBS.

Name	Sequence	Kd_{Tf} µM	Kd_{BSA} µM	Selectivity (Kd_{BSA}/Kd_{Tf})
Tf1	CGGGPFWWWP	1.21±0.06	1.98±0.33	1.63
Tf2	CGGGHKYLRW	0.90±0.25	2.61±0.38	2.9
Tf3	CGGGKRIFMV	6.64±0.08	1.70±0.46	0.25
Tf2-scr	CGGGKWHYLR	9.05±0.3	8.20±0.39	0.90

To assess the amount of aspecific adsorption to serum proteins, we also evaluated Kd towards BSA, in view of its high concentration in serum (up to 40 mg/mL) and known interaction with charged and hydrophobic peptides and biomolecules. We observed that both Tf1 and Tf2 bind to Tf with Kd in the low micromolar range, while Tf2-scr is markedly less efficient (Table 1). The higher efficiency of Tf2 compared with Tf2-scr evidences the pivotal role of amino acid sequence, and therefore of specific interactions, in determining binding to the protein target. The more hydrophobic Tf3 has a relatively low binding affinity (Kd= 6.64±0.08 µM), not far from the one of the control sequence Tf2-scr. Note that the relatively high Kd observed for Tf2 is in line with what observed for other protein-binding short peptide aptamers.[28,29] Additionally, it is actually sufficient to allow efficient interaction with Tf in biological media, since serum concentration of this protein is approximately 35 µM[30]. Not surprisingly, Tf2-scr shows nearly identical affinity towards BSA and Tf, while aspecific adsorption in the case of Tf3 was even greater than specific interaction with Tf. Conversely, both Tf1 and Tf2 have sensibly higher selectivity towards Tf (1.63 and 2.9 for Tf1 and Tf2, respectively, Table 1). This preliminary screening evidenced that Tf2 has both the highest Kd and best selectivity, so we selected only this sequence for further investigations.

Internalization assay in living cells

We sought to evaluate whether the observed binding properties of Tf2 could translate in efficient transferrin-mediated internalization. To this end, we labeled Tf2 with the commercial far red dye Atto-633 by standard thiol-maleimide coupling. Peptide was incubated with cultured adenocarcinoma pancreatic cells (Mia PaCa-2), a cell line expressing high levels of TfR,[31] in the presence of physiological (35 µM) levels of Tf. Internalization was assessed by confocal fluorescence microscopy (Figure 2) and compared with signal arising from fluorescent endocytosis markers (fluorescent transferrin for clathrin, dextran-70kDa-FITC for macropinocytosis, and caveolin-GFP for caveolae), to assess the internalization pathway. Indeed, specific transferrin mediated internalization should only occur by clathrin pathway, a typical route for TfR-mediated transport.[4,5] Other common internalization pathways, such as caveolae or micropinocytosis, would indicate occurrence of aspecific processes. As a negative control, we also evaluated the internalization of Tf2 in the absence of Tf and Tf2-scr in presence of physiological levels of Tf (Fig. S2). In both cases (i.e. either using Tf2 or Tf2-scr respectively in the absence or presence Tf) we observed minimal internalization, likely due to a minor contribution from aspecific interaction of peptides with serum proteins, or (less likely) by a low aspecific internalization. Conversely, when Tf2 was incubated with physiological levels of Tf, we observed extensive internalization upon short incubation times. Endocytosis

occurs essentially by clathrin mediated pathway (Pearson's Coefficient of 0.69±0.09, Fig. 3a-b). In keeping with the reported internalization pathway of transferrin, we also observed extensive colocalization at lysosomal level, with a Pearson's Coefficient of 0.59±0.08 (Fig. 3c). Conversely, colocalization with either macropinocytosis or caveolin markers (Fig 3d-e) was negligible (Pearson's Coefficient of 0.09±0.07 and 0.06±0.02 respectively); in these cases, internalization was smaller because of the lower levels of total Tf in the medium. Finally, we confirmed the absence of aspecific, passive internalization mechanisms by performing competitive inhibition experiments (Fig S3). Internalization of Tf2-Atto633 (1μM) was completely inhibited when the peptide was incubated either with a saturating excess of unlabeled Tf2 (1 mM) or with Tf (600 uM), confirming the absence of passive internalization mechanisms. Overall, these experiments confirmed that internalization of Tf2 occurs by transferrin-mediated endocytosis, with minimal aspecific uptake.

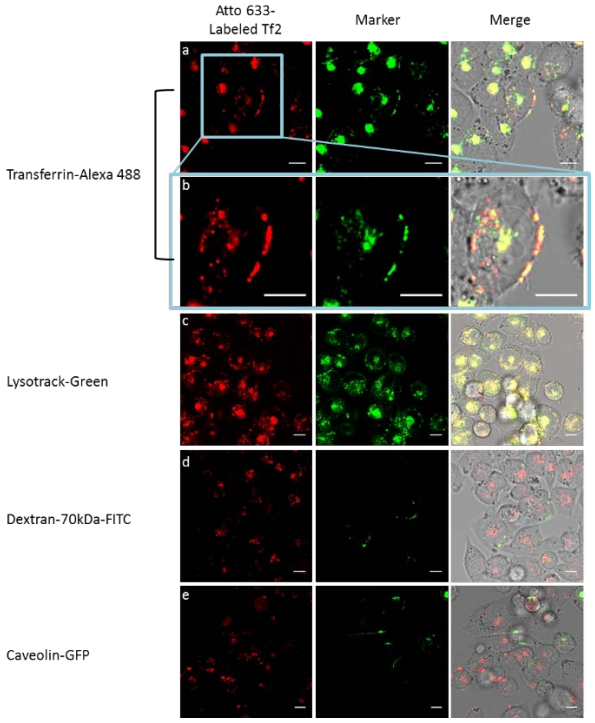

Figure 3: Internalization assay in adenocarcinoma pancreatic cells (Mia PaCa-2). Each peptide labelled with Atto633 (red channel) was incubated in cultured cells at concentration of 1 μM for 30 minutes at 37°C and 5% CO_2 and then internalization was monitored by confocal fluorescence microscopy. (a,b) Evaluation of clathrin-mediated endocytosis for Tf2-Atto633 incubated with hTransferrin-Alexa488, at concentration of 5 μM (green channel). (c) Confirmation of lysosomal internalization with Lysotracker Green at concentration of 70 nM (green channel). (d) Evaluation of macropinocytosis with Dextran(70kDa)-FITC, 1 mg/ml (green channel). (e) Analysis of caveolin-mediated endocytosis whit Mia PaCa-2 cells transfected with Caveolin-GFP fusion protein (green channel). Scale bars: 10 μm.

Internalization of gold nanoparticles conjugated to Tf2

Finally, we turned our attention to the ability of Tf2 to vehiculate nanostructured payloads in cells, to evaluate the effect of the protein corona modulation on the internalization of metal nanoparticles. To this end, we employed gold nanoparticles (30 nm), whose concentration in biological samples can be easily and precisely quantified by ICP-MS analysis. On the basis of our longstanding experience in the synthesis and functionalization of gold nanoparticles,[32,33] we derivatized the nanoparticles (Au-NPs) with two peptides: an already reported stabilizer (peptide N)[34], which prevents nanoparticle aggregation in solution, and a cognate of Tf2, PepN-Tf2 (**CLPFFD**PPPPHKYLRW). This peptide was designed using the base sequence of peptide N (in bold), and adding the already used proline spacer and Tf2. This design allows for highly efficient formation of a self-assembled monolayer (SAM), and leaves the targeting sequence projected outward -owing to the polyproline spacer- with minimal steric clash. Tf2 peptide was co-formulated in different proportions (0, 1 and 10% w/w) with peptide N (CLPFFD), and these mixtures were used to coat the surface of 30 nm gold nanoparticles, leading to **AuNP-0**, **AuNP-1**, and **AuNP-10**, respectively. Nanoparticles bearing more than 10% of **PepN-Tf2** are not stable in water solution, presumably due to the lowered surface charge; indeed, an immediate disappearance of the plasmon resonance at 530 nm and appearance of a purple color was observed upon addition of peptides, indicating the presence of large gold aggregates.[34] To evaluate aspecific protein adsorption and mimic bloodstream conditions, coated nanostructures were firstly incubated in pure human plasma in physiological conditions (1 h at 37°C) to promote formation of a protein corona. Immediately before incubation with cells (Mia PaCa-2), the nanoparticle suspension was diluted with DMEM to a final plasma concentration of 10%. After short incubation (30 minutes) and accurate washing with I_2/KI solution to remove externally adherent nanoparticles,[35] we quantified intracellular gold content by ICP-MS (Figure 4). Interestingly, we observed that internalization of gold nanoparticles is strongly dependent on the amount of **PepN-Tf2** (and hence of Tf2 sequences) on the surface. Indeed, internalization of **AuNP-10** was 44-fold greater compared with what observed for **AuNP-0**. The limited, yet not negligible, internalization of untargeted **AuNP-0** can be rationalized in view of the known ability of small nanoparticles to internalize in living cells even in the absence of targeting sequences, and could be minimized by suitable engineering of the SAM coating on the nanoparticle. These findings indicate that the presence of Tf2 significantly promotes receptor-mediated internalization of nanostructured payloads. Not surprisingly, internalization correlates with the percentage of targeting peptide Tf2 on the nanoparticle, which in turns is related to the amount of surface-bound transferrin. We verified that the presence of saturating (1 mM) amounts of unbound Tf2 partially inhibits nanoparticle internalization, in line with the already discussed competitive inhibition (Fig S3). However, the inhibitory effect is not complete, presumably owing to the increased apparent affinity which occurs upon multimerization on the surface of nanostructured systems.[36]

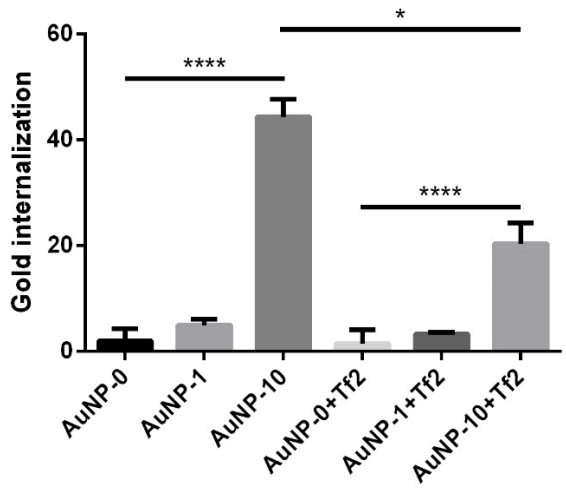

Figure 4: Internalization assay of gold nanoparticles conjugated with Tf2. Gold nanoparticles were coated with different percentage of PepN-Tf2 (0, 1 and 10% w/w) and incubated in human plasma 1 h at 37°C and then with Mia PaCa-2 cells for 1 h at 37°C in DMEM. Gold internalization was quantified by ICP-MS analysis on cells homogenate.

Composition analysis of the protein corona adsorbed on the surface of coated nanoparticles

Finally, we performed a proteomic analysis to fully characterize identity and amount of proteins adsorbed on the surface of nanoparticles upon incubation in a biological milieu. Peptide N is not optimized to confer antifouling properties; thus, it was expected that extensive protein adsorption would take place. Yet, the presence of a highly specific sequence such as Tf2 should promote differential adsorption of Tf. To this end, we prepared protein-coated nanoparticles by incubation with pure human plasma in physiological conditions (1 h at 37°C) as described above. After a washing and isolation step to remove loosely bound proteins, we analyzed adsorbed proteins by LC-MS/MS. We identified 68 proteins (see Supplementary material table 2) with 95% confidence level using Paragon algorithm. Transferrin was among the 15 most represented proteins on the nanoparticles surface (Table 2). Interestingly, comparative analysis evidenced higher amount of adsorbed Tf on the surface of **AuNP-1** and **AuNP-10** compared to **AuNP-0** (1.06 and 1.32 folds, respectively). Notably, there is an excellent agreement between the amount of adsorbed transferrin and internalization in cells, which is significative only in the case of **AuNP-10**. Note that in this case there is a large increase in internalization efficiency, if compared with the relatively small increase in adsorbed Tf (1.32 folds). It is tempting to explain this result with a better orientation of transferrin in the presence of Tf2 peptide, which promotes presentation of the active site of Tf towards the outer medium. This might increase the percentage of appropriately oriented Tf, which in turn could lead to significantly enhanced binding to TfR despite the formally similar concentration on the surface of the nanoparticle. It is worth noting that, along with transferrin, there are differences in some other representative proteins. Among the other represented proteins, which are actually common components of the "hard protein corona" formed on nanoparticles,[37] content of apolipoprotein (entries 11, 14) and fibrinogen (entries 12,13,15) decreases with increase of Tf2 peptide percentage, while immunoglobulin content does not show a clear trend, although a tendency to increase can be inferred from the available data. The overall decrease in aspecifically bound proteins could suggest a potential improvement of the biocompatibility of our system for potential therapeutic use, although the role of specific proteins should be further investigated. Finally, serum albumin content increases with Tf2 coverage, as expected in view of the reported interaction between HSA and Tf.[38] Note that this interaction could actually be the main responsible for the observed increase in HSA content on targeted nanoparticles. It is tempting to assume that the observed increase of HSA content does not reflect a direct increased interaction, but rather an indirect effect of the increased Tf content.

Table 2: Most abundant proteins identified by mass spectrometry on nanoparticle-protein corona complexes. Proteins are listed in decreasing order on the basis of their change on AuNP-10 compared to the control sample.

Entry	Accession	Protein Name	Fold Change (AuNP-10 over AuNP-0)	Fold Change (AuNP-1 over AuNP-0)
1	ALBU_HUMAN	Serum albumin	1.64	1.38
2	IGHG1_HUMAN	Ig gamma-1 chain C region	1.28	1.10
3	TRFE_HUMAN	Serotransferrin	1.32	1.06
4	FCN3_HUMAN	Ficolin-3	1.42	1.12
5	IGHM_HUMAN	Ig mu chain C region	1.34	1.20
6	IGKC_HUMAN	Ig kappa chain C region	4.57	1.54
7	IGHA1_HUMAN	Ig alpha-1 chain C region	0.97	1.13
8	LAC3_HUMAN	Ig lambda-3 chain C regions	0.69	1.04
9	ACTB_HUMAN	Actin, cytoplasmic 1	0.77	0.95
10	VTNC_HUMAN	Vitronectin	0.82	1.21
11	APOA1_HUMAN	Apolipoprotein A-I	0.93	0.78
12	FIBG_HUMAN	Fibrinogen gamma chain	0.27	0.61
13	FIBB_HUMAN	Fibrinogen beta chain	0.31	0.67
14	APOE_HUMAN	Apolipoprotein E	0.33	0.31
15	FIBA_HUMAN	Fibrinogen alpha chain	0.24	0.45

Conclusions

In conclusion, we developed a new Tf-binding peptide rationally designed by *in silico* selection. This approach allows design of sequences that bind to target proteins without affecting their biological function, and does not require production and purification of massive amounts of the target protein, thus being easily exploitable for the development of sequences against rare or unstable proteins. The obtained peptide (Tf2) shows good binding efficiency towards its target with limited aspecific protein adsorption, and is efficiently internalized in cells by transferrin-mediated endocytosis. Furthermore, Tf2 can be conjugated to nanostructured compounds such as gold nanoparticles, and effectively promotes internalization in the presence of physiological (i.e. plasma) level of transferrin. Finally, we demonstrated, by means of proteomic analyses, that the targeting peptide Tf2 modifies the protein corona composition on gold nanoparticles upon incubation in human plasma, thus opening new avenues in the development of nanostructures that acquire selectivity by spontaneous adsorption of specific serum/plasma proteins with controlled orientation. Further studies are in progress to improve the proposed algorithm to better filtering against aspecific binding, evaluate the potential of this sequence to the targeted delivery of therapeutics *in vitro* and *in vivo*, and develop new binding sequences against biologically relevant molecules.

MATERIALS AND METHODS

All chemicals were purchased from Sigma Aldrich unless otherwise specified, and were used as received.

Identification of binding pocket

Binding pockets on the transferrin were predicted using Fpocket[24] and ranked according to their Voronoi volume (Fig 1B). Only one pocket was identified as being wide enough to accommodate a hexapeptide. Moreover, the same binding pocket was present with minor changes in both the unbound and bound transferrin.

Sequence design and QSAR analysis

The in silico design procedure consists of a series of iterative steps, in which a regression model for the prediction of the physico-chemical requirement of binding is inferred from molecular dynamic simulations. As the iterative procedure goes on, the model is further optimized with information gathered from previous steps. In the first iteration, hexapeptides are randomly generated and molecular dynamic simulations (see next paragraph for details) are performed in order to associate a theoretical binding energy to each tested sequence. From the second iteration on, the information generated by MD simulations is used to build a regression model describing the physico-chemical requirements for binding. Peptide sequences are encoded into quantitative structure-activity relationship (QSAR) descriptors by using global features (net charge, isoelectric point) and topological features (auto- and cross-correlation of variables) as previously described[27] (Table S1). In this study, the Support Vector Machine for regression (SMOReg), is used as implemented in the software suite WEKA[39]. Model performance was measured with a 10-fold cross-validation analysis, where the peptide dataset was divided into 10 parts - 9 parts for model learning (training) and the remaining part for validation (testing). The regression performance is evaluated by the Pearson correlation coefficient.

A class of genetic algorithms called multi-objective evolutional algorithms (MOEA)[40] is used in combination with the regression model to find a set of candidate sequences with a predicted high binding energy and at the same time minimize the number of charged/hydrophobic amino acids. In particular, hydrophobicity was measured with the Consensus Hydrophobicity Scale (CCS).[26] This measure of hydrophobicity is based on a set of literature base scales, normalised and filtered by different methods. In order to avoid overfitting of candidate sequences, and exploring a wider space of the physico-chemical features, at each iteration 30% of the sequence library was designed by MOEA, while the remaining 70% was randomly designed. In this work, 100 peptides were designed and virtually docked at each iteration, for a total of 10 iterative steps. The top three peptides (Tf1, Tf2, Tf3) obtained at the last iteration by the MOEA were selected to be experimentally tested. Moreover, a scrambled version of Tf2 was generated in order to test for specificity.

Molecular dynamic simulations

Starting from a list of hexapeptide sequences, a library of all-atom (AA) structures is generated by MODELLER[41] using an extended hexapeptide as template. For each structure, an initial CG protein-peptide complex is assembled by placing the AA peptide in the target pocket and converting the resulting system to a CG MARTINI model with *martinize.py* script. The system is then minimized with 1000 step steepest descendent minimization, followed by an equilibration of 4ps. The temperature was maintained at 298K by coupling the system to a Nosè − Hoover thermostat. This allows resolving steric clashes due to the initial approximate positioning of hexapeptides into the binding pocket. The equilibrated complex is then backmapped to AA by MARTINI *backmapping* script using the CHARMM force field.[42] The binding free energy is estimated at the last frame of the 4ps simulations using the molecular mechanics Poisson-Boltzmann surface area (MM-PBSA) method as implemented in g_mmpbsa[25]. This procedure is repeated 10 times for each peptide, in order to verify its reproducibility and increase statistics.

Analysis of docked poses

Selected peptides (Tf1, Tf2, Tf2-scrambled, Tf3) where subjected to 1ns molecular dynamics simulations within the Tf pocket. Molecular dynamics simulations have been performed as described hereafter. The system was solvated with TIP3P water molecules ensuring a minimum distance to the box edge of 1 nm. A steepest-descent minimization was applied to relax the solvent molecules. The system was thermalized up to 300 K using a V-rescale thermostat ($\tau_t = 0.1$) in the canonical ensemble. One nanosecond simulation was then performed in the normal temperature and pressure (NPT: p=1 bar, T=300 K) statistical ensemble coupling the system with a Parrinello-Rahman barostat ($\tau_p = 2$). All bonds were constrained with LINCS[43], allowing to use a time step set of 2 fs. Periodic boundary conditions were applied to the systems in all directions. PME method[44] was used to evaluate long-range electrostatic interactions (pme order=4, fourier spacing=0.12), and a cutoff of 10 Å was used to account for the van der Waals interactions. Coordinates of the systems were collected every 2 ps. Simulations were performed using GROMACS 5.0[45] using the CHARMM force field. Hierarchical cluster analysis was then applied to the equilibrium

trajectories using the silhouette method for determining the best number of clusters. The centroid of the most populated cluster was used as representative docked pose.

Peptide synthesis and purification

All peptides were prepared by solid-phase synthesis using Fmoc chemistry on an automatic Liberty Blue Peptide Synthesizer with an integrated microwave system (CEM, North Carolina, USA). HPLC analysis and purification were performed on a Dionex Ultimate 3000 PLC system with autosampler. Crude peptides were purified by RP-HPLC on a Jupiter 4 µm Proteo 90 Å column (250×10 mm; Phenomenex) using these solvents: water:TFA 100:0.01 v/v (eluent A)/acetonitrile:water:TFA 95:5:0.01 v/v (eluent B), flux 5 ml/min. The identity of purified product was confirmed by electrospray mass spectroscopy, using an API3200QTRAP Hybrid Triple Quadrupole/Linear Ion Trap (ABSciex, Foster City, California, USA).

Conjugation with fluorophores

All peptides were conjugated with the Atto633-maleimide (ATTO-TEC GmbH, Germany) fluorophore by means of maleimide-thiol coupling chemistry. The reaction was conducted in Hepes buffer (20 mM, pH= 7.2) under stirring at 25°C at least for 2 hours. Analytical evaluation of labeling reaction and purity of the labeled peptide was performed on a Jupiter Proteo 90 Å column (4µm, 250×10 mm; Phenomenex) using these solvents: water:TFA 100:0.01 v/v (eluent A)/acetonitrile:water:TFA 95:5:0.01 v/v (eluent B), flux 1 ml/min. The identity of purified product was confirmed by electrospray mass spectroscopy.

QCM-D measurements

Quartz crystal microbalance measurements were carried out with a dissipative QCM (Q-Sense, Gothenburg, Sweden) using AT-cut 5 MHz quartz crystals coated with a 3–100 nm thick layer of gold (Biolin Scientific, Stockholm, Sweden) at 25°C. Before use, they were cleaned with ethanol and dried under nitrogen flow. Experiments were carried out in stopped-flow mode using a syringe pump operating at a flow rate of 100 µl/min and PBS as carrier buffer. Data were simultaneously acquired at the fundamental frequency F of 5 MHz (N = 1) and several overtone frequencies (15, 25, 35, 45, and 55 MHz, i.e. N = 3, 5, 7, 9 and 11). The curves shown in Fig. S1 are those obtained with the ninth harmonics (45 MHz). We used each peptide at a concentration of 10 µM and increasing concentration of hTransferrin or BSA in a range from 1 to 50 µM.

Cell culture

Human adenocarcinoma pancreatic cells (Mia PaCa-2) were purchased from the American Type Culture Collection (ATCC) and were maintained in Dulbecco's Modified Eagle Medium (DMEM) from Invitrogen (Carlsbad, CA). Growth medium was supplemented with 10% fetal bovine serum (FBS), 4 mM L-Glutamine, 1 mM Sodium Pyruvate, 100 U/ml penicillin and 100 mg/ml streptomycin (Invitrogen). Cells were maintained at 37°C in a humidified 5% CO_2 atmosphere.

Confocal microscopy

Cells were seeded 24 h before the experiments into glass-bottom petri dish (WillCo-dish GWSt-3522) to reach 80-90% of confluence. Incubation of peptides was performed for 30 minutes at 37°C or 4°C, 5% CO_2 in DMEM with 10% FBS at a final concentration of 1 µM in a total volume of 200 µl. After incubation, cells were washed twice with PBS, fresh medium was added and the samples were analyzed by confocal microscopy. We tested all type of endocytosis with the same incubation condition but adding different fluorescent markers together with the peptides. For clathrin-mediated endocytosis we used 5 µM of hTransferrin-Alexa488 and we added the right amount of unlabeled hTF to a total concentration of 35 µM, comparable with the one in the human plasma. In the same experimental conditions, colocalization of the peptide with Lysotracker Green (final concentration: 70 nM) confirmed this internalization pathway and final compartmentalization in lysosomes. For macropinocytosis we used 1 mg/ml of Dextrans (70kDa) labeled with FITC and for caveolin-mediated endocytosis we used Mia PaCa-2 cells transfected with caveolin-GFP. In both cases the amount of Tf was due only to the FBS added to the medium (approximately 3 µM). Cells were imaged using a Leica TCS SP5 SMD inverted confocal microscope (Leica Microsystems AG) interfaced with Ar and DPSS laser for excitation at 488 nm and 561 nm respectively. Cells were mounted in a thermostated chamber at 37°C (Leica Microsystems) and viewed with a 40x 1.5 NA oil immersion objective (Leica Microsystems). The pinhole aperture was set to 1.0 Airy. All images were analyzed using ImageJ software 1.48v and colocalization was evaluated using JACoP plugin. The final value of Pearson's Coefficient is an average obtained from the analysis of 10 images taken with the same magnification for each experiment.

Synthesis of gold nanoparticles and peptide conjugation

Gold seeds were prepared[46] by refluxing for 30 min 100 mL of aqueous solution of $HAuCl_4$ (1 mM) with sodium acrylate (24 mM). The reaction produced a deep-red colloid characteristic of 14 nm spheres. For the second step all the seed solution was mixed to 15 mL of 25 mM $HAuCl_4$ solution and diluted in 845 mL of MilliQ water. The mixture was brought to pH = 7 and 40 mL of 0.5 M acrylic acid solution was added. After 3 days at 22 °C under continuous stirring; the reaction produced a wine-red solution of 30 ± 1.7 nm gold nanoparticles at a 0.5 nM (2.92×10^{11} NP ml^{-1}) concentration. For peptide conjugation, 1 ml of the above colloid was centrifuged for 5 minutes at 13,000 rpm and resuspended in 900 µl of DMF. Starting from solution of 1 mM for both peptides, three different peptide solutions were made (only peptide N, peptide N + peptide N-Tf2 99:1 and peptide N + peptide N-Tf2 90:10) to a final volume of 100 µl, which was added to nanoparticles solution and stirred for 90 minutes at 4°C. After incubation, conjugated nanoparticles were washed thrice with TEA buffer and resuspended in 100 µl of the same buffer.

Plasma incubation and isolation of nanoparticles with protein corona

Conjugated nanoparticle suspensions (100 µl) were incubated with 250 µl of human plasma, in a total volume of 350 µl and were stirred for 1 h at 37 °C. After incubation samples were centrifuged at 4°C to pellet the nanoparticle-protein complex. The pellets were washed thrice with PBS-EDTA buffer (PBS 1X, EDTA 1 mM and pH = 7.5) and resuspended in PBS-EDTA buffer to a final volume of 20 µl. Each sample was prepared in double for the internalization assay by ICP-MS and for proteomics analysis by LC-MS/MS.

Gold nanoparticles internalization in living cells

In order to verify the targeting capabilities of the conjugated nanoparticles produced as above described, gold was

quantified by means of ICP-MS after incubation in living cells. Cells were seeded 24 h before experiments in a 12-well plate to reach 80-90% of confluence. Nanoparticles were maintained in human plasma from healthy donors for 1 h at 37°C under continuous stirring and then diluted with serum-free DMEM to obtain a final concentration of plasma of 10%. The solution was administered to Mia-PaCa-2 and incubated for 1 h. After this time cells were washed once with PBS and once with a I_2/KI solution (ratio 1:6 with I_2 at a final concentration of 0.34 mM) for 5 minutes to eliminate nanoparticles attached on cell surface.[35] Then we discarded the supernatant, we washed once with PBS and we digested the cells with 0.2 ml of aqua regia. Samples were analyzed by ICP-MS (7700 series ICP-MS, Agilent Technologies) to quantify gold. Untreated cells were processed, digested, and used to determine blank signal. This contribution was subtracted to the signal obtained for treated cells. Data in Fig. 4 represent the average of three independent experiments and error bars state the standard error. A one-way ANOVA and t-test were used to assess differences in the data with $p \leq 0.05$, considered as statistically significant.

Nano LC-MS/MS SWATH™ proteomics analysis

Particles with their corona were suspended in 100 µl of 25 mM Ammonium Bicarbonate/ 10% Acetonitrile (ACN, Romil, UK) and vortexed. 50 µl of suspension were diluted again to 100 µl, reduced 30 min with 5 mM Dithiothreitol @ 80°C, alkylated adding 10 mM of Iodoacetamide at 37°C for 20 min and digested overnight with 0.6 mg/ml of trypsin (Roche, Germany) at 37°C. Peptide solutions were acidified and centrifuged for 10 min at 10°C and 13000 rpm in order to discard nanoparticles; supernatant was loaded on a C18 cartridge and filtered on a 0.22 µm filter. Eluate was evaporated in a SpeedVac (Savant) and diluted to 50 µL of 2% ACN/0.1% Formic Acid (FA); 5 µl of each sample were injected for library and 5 µl in duplicate for SWATH analysis.

Chromatographic separation of eluted peptides was performed using a nano-HPLC system (Eksigent, ABSciex, USA). A first load step pre-concentrated the sample in a pre-column cartridge (PepMap-100 C18 5 µm 100 A, 0.1 x 250 mm, Thermo Scientific, USA) and then peptides were separated in a C18 PepMap-100 column (3 µm, 75 µm x 150 mm, Thermo Scientific, USA) at a flow rate of 300 nl min^{-1}. Runs were performed with eluent A (Ultrapure water, 0.1% FA) in a 70 min linear gradient from 5 to 40% of eluent B (ACN/0.1% FA) followed by 10 min of a purge step and 20 min re-equilibration step. Peptides eluted from chromatography were directly analysed using a TripleTOF™ 5600 mass spectrometer (ABSciex, USA) equipped with a DuoSpray™ ion source (ABSciex, USA). Data for protein library were acquired in IDA (information dependent acquisition) mode, survey scans were acquired in 250 ms and 25 product ion scans. MS/MS data were processed with ProteinPilot™ Software (ABSciex, USA) using SwissProt database for Homo sapiens (updated to May 2016). The false discovery rate (FDR) analysis was set to a confidence level of 95%. The label free comparative analysis of samples was performed on data acquired using SWATH™ method for shotgun data independent MRM quantification, loaded into PeakView™ Software (ABSciex, USA) with MS/MS(ALL) with SWATH™ Acquisition MicroApp 2.0 and MarkerView™ (ABSciex, USA). Retention time alignment was obtained using selected peptides (top confidence and top level transitions) from top score protein. Processing settings were: 7 peptides per protein, 7 transitions per peptide, 74% peptide confidence (according to Paragon algorithm result) and 5% FDR; XIC options: extraction window 10 min, width 50 ppm and 0.1 Da. Normalization was done using a global normalization of profiles (total protein content) on chromatographic area, then protein intensity from serum "blank" sample was subtracted to respective sample protein intensity. Blank corrected data were compared to evidence fold change across samples.

SUPPORTING INFORMATION AVAILABLE

List of descriptors for *in silico* peptide analysis, QMC measurements, additional microscopy images and tables of proteomics analysis.

ACKNOWLEDGMENTS

The authors thank Mr. Domenico Cassano for useful discussions.

REFERENCES

(1) Communication, S. (2006) Gold nanoparticles : a new X-ray contrast agent *79*, 248–253.

(2) Ren, W. H., Chang, J., Yan, C. H., Qian, X. M., Long, L. X., He, B., Yuan, X. B., Kang, C. S., Betbeder, D., Sheng, J., and Pu, P. Y. (2010) Development of transferrin functionalized poly(ethylene glycol)/poly(lactic acid) amphiphilic block copolymeric micelles as a potential delivery system targeting brain glioma. *J. Mater. Sci. Mater. Med. 21*, 2673–2681.

(3) Eck, W., Craig, G., Sigdel, A., Ritter, G., Old, L. J., Tang, L., Brennan, M. F., Allen, P. J., and Mason, M. D. (2008) Antibodies as Targeted Labeling Agents for Human Pancreatic Carcinoma Tissue. *ACS Nano 2*, 2263–2272.

(4) Porciani, D., Tedeschi, L., Marchetti, L., Citti, L., Piazza, V., Beltram, F., and Signore, G. (2015) Aptamer-Mediated Codelivery of Doxorubicin and NF-κB Decoy Enhances Chemosensitivity of Pancreatic Tumor Cells. *Mol. Ther. Acids 4*, e235.

(5) Porciani, D., Signore, G., Marchetti, L., Mereghetti, P., Nifosì, R., and Beltram, F. (2014) Two Interconvertible Folds Modulate the Activity of a DNA Aptamer Against Transferrin Receptor. *Mol. Ther. Acids 3*, e144.

(6) Weissleder, R., Kelly, K., Sun, E. Y., Shtatland, T., and Josephson, L. (2005) Cell-specific targeting of nanoparticles by multivalent attachment of small molecules. *Nat. Biotechnol. 23*, 1418–1423.

(7) Monopoli, M. P., Walczyk, D., Campbell, A., Elia, G., Lynch, I., Bombelli, F. B., Dawson, K. a., Baldelli Bombelli, F., and Dawson, K. a. (2011) Physical-chemical aspects of protein corona: relevance to in vitro and in vivo biological impacts of nanoparticles. *J. Am. Chem. Soc. 133*, 2525–2534.

(8) Nel, A. E., Mädler, L., Velegol, D., Xia, T., Hoek, E. M. V, Somasundaran, P., Klaessig, F., Castranova, V., and Thompson, M. (2009) Understanding biophysicochemical interactions at the nano-bio interface. *Nat. Mater. 8*, 543–557.

(9) Salvati, A., Pitek, A. S., Monopoli, M. P., Prapainop, K., Bombelli, F. B., Hristov, D. R., Kelly, P. M., Åberg, C., Mahon, E., and Dawson, K. a. (2013) Transferrin-functionalized nanoparticles lose their targeting capabilities when a biomolecule corona adsorbs on the surface. *Nat. Nanotechnol. 8*, 137–43.

(10) Caracciolo, G., Cardarelli, F., Pozzi, D., Salomone, F., Maccari, G., Bardi, G., Capriotti, A. L., Cavaliere, C., Papi, M., and Laganà, A. (2013) Selective targeting capability acquired with a protein corona adsorbed on the surface of 1,2-dioleoyl-3-trimethylammonium propane/dna nanoparticles. *ACS Appl. Mater. Interfaces 5*, 13171–13179.

(11) Wilson, D. R., and Finlay, B. B. (1998) Phage display : applications , innovations , and issues in phage and host biology *329*, 313–329.

(12) Coates, P. J., and Hall, P. A. (2003) The yeast two-hybrid system for identifying protein – protein interactions 4–7.

(13) Daniels, T. R., Delgado, T., Rodriguez, J. a., Helguera, G., and Penichet, M. L. (2006) The transferrin receptor part I: Biology and targeting with cytotoxic antibodies for the treatment of cancer. *Clin. Immunol. 121*, 144–158.

(14) Daniels, T. R., Bernabeu, E., Rodríguez, J. A., Patel, S., Kozman, M., Chiappetta, D. A., Holler, E., Ljubimova, J. Y., Helguera, G., and Penichet, M. L. (2012) The transferrin receptor and the targeted delivery of therapeutic agents against cancer. *Biochim. Biophys. Acta 1820*, 291–317.

(15) Shindelman, J. E., Ortmeyer, A. E., and Sussman, H. H. (1981) Demonstration of the Transferrin Receptor in Human Breast Cancer Tissue. Potential Marker For Identifying Dividing Cells. *Int. J. Cancer*.

(16) Ryschich, E., Huszty, G., Knaebel, H. P., Hartel, M., Büchler, M. W., and Schmidt, J. (2004) Transferrin receptor is a marker of malignant phenotype in human pancreatic cancer and in neuroendocrine carcinoma of the pancreas. *Eur. J. Cancer 40*, 1418–1422.

(17) Łubgan, D., Jóźwiak, Z., Grabenbauer, G. G., and Distel, L. V. R. (2009) Doxorubicin-transferrin conjugate selectively overcomes multidrug resistance in leukaemia cells. *Cell. Mol. Biol. Lett. 14*, 113–127.

(18) Head, J. F., Wang, F. E. N., and Elliott, R. L. (1997) Drugs That Interfere With Iron Metabolism in Cancer. *Science (80-.). 37*, 147–169.

(19) O'Keefe, D. O., and Draper, R. K. (1985) Characterization of a transferrin-diphtheria toxin conjugate. *J. Biol. Chem. 260*, 932–7.

(20) Pun, S. H., Tack, F., Bellocq, N. C., Cheng, J., Grubbs, B. H., Jensen, G. S., Davis, M. E., Brewster, M., Janicot, M., Janssens, B., Floren, W., and Bakker, A. (2004) Targeted delivery of RNA-cleaving DNA enzyme (DNAzyme) to tumor tissue by transferrin-modified, cyclodextrin-based particles. *Cancer Biol. Ther. 3*, 641–650.

(21) Kursa, M., Walker, G. F., Roessler, V., Ogris, M., Roedl, W., Kircheis, R., and Wagner, E. (2003) Novel shielded transferrin-polyethylene glycol-polyethylenimine/DNA complexes for systemic tumor-targeted gene transfer. *Bioconjug. Chem. 14*, 222–231.

(22) Monticelli, L., Kandasamy, S. K., Periole, X., Larson, R. G., Tieleman, D. P., and Marrink, S.-J. (2008) The MARTINI Coarse-Grained Force Field: Extension to Proteins. *J. Chem. Theory Comput. 4*, 819–834.

(23) Noinaj, N., Easley, N. C., Oke, M., Mizuno, N., Gumbart, J., Boura, E., Steere, A. N., Zak, O., Aisen, P., Tajkhorshid, E., Evans, R. W., Gorringe, A. R., Mason, A. B., Steven, A. C., and Buchanan, S. K. (2012) Structural basis for iron piracy by pathogenic Neisseria. *Nature 483*, 53–58.

(24) Le Guilloux, V., Schmidtke, P., and Tuffery, P. (2009) Fpocket: An open source platform for ligand pocket detection. *BMC Bioinformatics 10*, 168.

(25) Kumari, R., Kumar, R., and Lynn, A. (2014) g_mmpbsa--a GROMACS tool for high-throughput MM-PBSA calculations. *J. Chem. Inf. Model. 54*, 1951–62.

(26) Tossi A., Sandri L., G. A. (2002) New consensus hydrophobicity scale extended to non-proteinogenic amino acids, in *Peptides 2002: Proceedings of the 27th European Peptide Symposium*, pp 416–417.

(27) Maccari, G., Di Luca, M., Nifosí, R., Cardarelli, F., Signore, G., Boccardi, C., and Bifone, A. (2013) Antimicrobial peptides design by evolutionary multiobjective optimization. *PLoS Comput. Biol. 9*, e1003212.

(28) Binétruy-Tournaire, R., Demangel, C., Malavaud, B., Vassy, R., Rouyre, S., Kraemer, M., Plouët, J., Derbin, C., Perret, G., and Mazié, J. C. (2000) Identification of a peptide blocking vascular endothelial growth factor (VEGF)-mediated angiogenesis. *EMBO J. 19*, 1525–1533.

(29) Oldenburg, K. R., Loganathan, D., Goldstein, I. J., Schultz, P. G., and Gallop, M. a. (1992) Peptide ligands for a sugar-binding protein isolated from a random peptide library. *Proc. Natl. Acad. Sci. U. S. A. 89*, 5393–5397.

(30) Vet-, B., and Wp, S. (1991) Growth of Vibrio vulnificus in Serum from Alcoholics: Association with High Transferrin Iron Saturation Colleagues- *164*, 1030–1032.

(31) Camp, E. R., Wang, C., Little, E. C., Watson, P. M., Pirollo, K. F., Rait, A., Cole, D. J., Chang, E. H., and Watson, D. K. (2013) Transferrin receptor targeting nanomedicine delivering wild-type p53 gene sensitizes pancreatic cancer to gemcitabine therapy. *Cancer Gene Ther. 20*, 222–228.

(32) Voliani, V., Signore, G., Vittorio, O., Faraci, P., Luin, S., Peréz-Prieto, J., and Beltram, F. (2013) Cancer phototherapy in living cells by multiphoton release of doxorubicin from gold nanospheres. *J. Mater. Chem. B 1*, 4225.

(33) Cassano, D., Santi, M., Cappello, V., Luin, S., Signore, G., and Voliani, V. (2016) Biodegradable passion fruit-like nano-architectures as carriers for cisplatin prodrug. *Part. Part. Syst. Charact. 3*, 818–824.

(34) Voliani, V., Luin, S., Ricci, F., and Beltram, F. (2010) Single-step bifunctional coating for selectively conjugable nanoparticles. *Nanoscale 2*, 2783–2789.

(35) Cho, E. C., Xie, J., Wurm, P. A., and Xia, Y. (2009) Understanding the Role of Surface Charges in Cellular Adsorption versus Internalization by Selectively Removing Gold Nanoparticles on the Cell Surface with a I 2 / KI Etchant 2009.

(36) Mammen, M., Choi, S.-K., and Whitesides, G. M. (1998) Polyvalent Interactions in Biological Systems: Implications for Design and Use of Multivalent Ligands and Inhibitors. *Angew. Chem. Int. Ed. 37*, 2754–2794.

(37) Lundqvist, M., Stigler, J., Elia, G., Lynch, I., Cedervall, T., and Dawson, K. A. (2008) Nanoparticle size and surface properties determine the protein corona with possible implications for biological impacts. *Proc. Natl. Acad. Sci. U. S. A. 105*, 14265–70.

(38) Chamani, J., Vahedian-Movahed, H., and Saberi, M. R. (2011) Lomefloxacin promotes the interaction between human serum albumin and transferrin: A mechanistic insight into the emergence of antibiotic's side effects. *J. Pharm. Biomed. Anal. 55*, 114–124.

(39) Hall, M., Frank, E., Holmes, G., Pfahringer, B., Reutemann, P., and Witten, I. H. (2009) The WEKA data mining software. *ACM SIGKDD Explor. Newsl. 11*, 10.

(40) Solmajer, T., and Zupan, J. (2004) Optimization algorithms and natural computing in drug discovery. *Drug Discov. Today Technol. 1*, 247–252.

(41) Sali, A., and Blundell, T. L. (1993) Comparative protein modelling by satisfaction of spatial restraints. *J. Mol. Biol. 234*, 779–815.

(42) Vanommeslaeghe, K., Hatcher, E., Acharya, C., Kundu, S., Zhong, S., Shim, J., and Darian, E. (2009) CHARMM General Force Field : A Force Field for Drug-Like Molecules Compatible with the CHARMM All-Atom Additive Biological Force Fields.

(43) Hess, B., Bekker, H., Berendsen, H. J. C., and Fraaije, J. G. E. M. (1997) LINCS : A Linear Constraint Solver for Molecular Simulations *18*, 1463–1472.

(44) Darden, T., York, D., Pedersen, L., Darden, T., York, D., and Pedersen, L. (1993) Particle mesh Ewald : An Nlog (N) method for Ewald sums in large systems Particle mesh Ewald : An N -log (N) method for Ewald sums in large systems *10089*.

(45) James, M., Murtola, T., Schulz, R., Smith, J. C., Hess, B., and Lindahl, E. (2015) ScienceDirect GROMACS : High performance molecular simulations through multi-level parallelism from laptops to supercomputers *2*, 19–25.

(46) Hussain, I., Brust, M., Papworth, A. J., and Cooper, A. I. (2003) Preparation of acrylate-stabilized gold and silver hydrosols and gold-polymer composite films. *Langmuir 19*, 4831–4835.